Available online at www.sciencedirect.com
ScienceDirect
Earth and Planetary Science Letters 258 (2007) 500–515
EPSL
www.elsevier.com/locate/epsl

Quantifying sand provenance and erosion (Marsyandi River, Nepal Himalaya)

Eduardo Garzanti [a,*], Giovanni Vezzoli [a,1], Sergio Andò [a,1], Jérôme Lavé [b,2], Mikaël Attal [b,2], Christian France-Lanord [c,3], Peter DeCelles [d,4]

[a] *Laboratorio di Petrografia del Sedimentario, Dipartimento di Scienze Geologiche e Geotecnologie, Università di Milano-Bicocca, 20126 Milano, Italy*
[b] *Laboratoire de Géodynamique des Chaînes Alpines, UMR CNRS 5025, BP53, 38041 Grenoble Cedex 09, France*
[c] *CRPG-CNRS, 15, rue Notre Dame des Pauvres, 54501 Vandoeuvre-lès-Nancy, France*
[d] *Department of Geosciences, University of Arizona, Tucson, AZ 85721, USA*

Received 5 February 2007; received in revised form 28 March 2007; accepted 2 April 2007
Available online 11 April 2007
Editor: M.L.Delaney

Abstract

We use petrographic and mineralogical data on modern sediments to investigate erosion patterns in the Marsyandi basin of the central Himalaya, a privileged natural laboratory in which a series of multidisciplinary geomorphological, sedimentological, geochemical and geochronological studies have been recently carried out to unravel the interrelationships between tectonic, climatic and sedimentary processes in high-relief orogenic belts. Although relative erosion patterns are effectively constrained by analyses of replicate samples along six successive tracts of the Marsyandi River, uncertainties are caused by potential compositional variation between the monsoon and post-monsoon season. Estimates of erosion rates are significantly affected by poor knowledge of total sediment flux through the basin.

Our results support focused erosion of the southern, tectonically-lower part of the Greater Himalaya in the hangingwall of the MCT Zone, where the summer monsoon reaches its peak intensity (up to 5 m/a), and sediment yields and erosion rates reach 14,100±3400 t/km^2 and 5.1±1.2 mm/a. Erosion rates sharply decrease southward in low-relief Lesser Himalayan units (1.6±0.6 mm/a), and also progressively decrease northwards in the high-altitude, tectonically-upper part of the Greater Himalaya, where rainfall decreases rapidly to <2 m/a. Even areas of extreme topography such as the Manaslu Granite are characterized by relatively low erosion rates (2.4±0.9 mm/a), because precipitations become too scarce to feed significant ice flux and glacial activity. Monsoonal rainfall decreases further to <0.5 m/a in the Tethys Himalayan zone farther north, where erosion rates are ~ 1 mm/a. Coupling between erosion and peak monsoonal rainfall along the southern front of the Greater Himalaya is consistent with both channel-flow models of tectonic extrusion

* Corresponding author. Tel.: +39 2 64482088; fax: +139 2 64484273.
E-mail addresses: eduardo.garzanti@unimib.it (E. Garzanti), giovanni.vezzoli@unimib.it (G. Vezzoli), sergio.ando@unimib.it (S. Andò), Jerome.Lave@ujf-grenoble.fr (J. Lavé), mikael.attal@ed.ac.uk (M. Attal), cfl@crpg.cnrs-nancy.fr (C. France-Lanord), decelles@geo.arizona.edu (P. DeCelles).
[1] Tel.: +39 2 64482088; fax: +139 2 64484273.
[2] Now at Institute of Earth Science, School of GeoSciences, University of Edinburgh, West Mains Road, Edinburgh EH9 3JW, Scotland. Tel.: +33 0476635919; fax: +33 0476514058.
[3] Tel.: +33 383 594220: fax: +33 383 511798.
[4] Tel.: +1 520 6214910: fax: +1 520 6212672.

doi:10.1016/j.epsl.2007.04.010

and tectonic uplift above a mid-crustal ramp. Altitude and relief are not the principal factors controlling erosion, and the central Nepal eight-thousanders may be viewed as topographic anomalies in cold desert climate at the southern edge of the Tibetan rain shadow.

Keywords: modern sands; bulk petrography; sediment budgets; erosion rates; monsoon season; Tethys Himalaya; Greater Himalaya; Lesser Himalaya; collision orogens

1. Introduction

The traditional view that tectonic processes create topographic relief, which in turn controls precipitation distribution, fluvial discharge, erosion patterns and sediment evacuation has been recently challenged by the apparently more extravagant idea that the opposite may be true as well, and that climatically-driven erosion at the Earth's surface can govern tectonic deformation, in a feedback loop that finally induces even metamorphism and melting in the deep crust [1–4]. To improve on our current understanding of how mountain ranges are uplifted and worn away, we must detangle first the complex interplay between tectonic, climatic, and geomorphological processes [5–7], and clarify if, why, and how orogenic systems evolve towards an equilibrium between endogenous and exogenous geological forces [8,9]. In order to shed light on this actively debated conundrum [10–12], coupled geodynamic-erosion models can be tested against comprehensive data-sets collected in active settings such as the Himalayan Range, where abrupt gradients in precipitation, erosion, and deformation produce signals that rise well above the noise of natural systems [13–15].

In recent years, the Marsyandi catchment in central Nepal has become a privileged natural laboratory in which to investigate the relative impact of climatic and tectonic processes on erosion in high-relief orogenic belts. In order to quantify patterns of erosion at different spatial and temporal scales, a network of meteorological stations were installed [16–18], digital topography and geomorphological analyses were carried out [19 20], and water and sediment chemistry [21–24] as well as sediment-transport and gravel bedload were studied [25,26]. Several geochronological techniques on bedrock and sediments, including zircon and apatite fission-track and (U–Th)/He analyses [14,27,28], cosmogenic radionuclides [20,29,30], Ar/Ar on detrital muscovite [31–33], and U/Pb on detrital zircons [34,35] were also applied.

In spite of such extensive multidisciplinary studies, detailed bulk petrography and heavy-mineral information on sand-sized sediments was lacking so far. Moreover, rates and patterns of erosion inferred from these different techniques diverge widely. Whereas a majority of studies support focused erosion of the Greater Himalaya [13,14,21], recent analyses suggested instead erosion rates up to three-times faster in the upper Lesser Himalaya [34,35]. The reasons for such discrepancies must be investigated to improve on our understanding of the orogenic processes active in the Nepal Himalaya.

In this study we carry out high-resolution petrographic and heavy-mineral analyses on 36 modern sands collected in the Marsyandi catchment, and assess the relative abundance of every detrital species in each tributary or trunk river tract. This data base allows us to quantify the relative contributions from each tributary and geological unit to the overall Marsyandi load, and thus to evaluate sediment yields and erosion patterns in distinct parts of its basin. The calculated denudation rates can be compared with patterns of tectonic uplift and monsoonal precipitation, in order to investigate possible coupling between erosion and climatic or tectonic processes. Detailed quantitative data on bulk sediment composition also represent a fundamental pre-requisite to compare, correctly interpret, and integrate the various pieces of information achieved by applying different geochronological or geochemical techniques on single mineral grains (e.g., fission-tracks on detrital apatites, Ar/Ar on detrital muscovites, U/Pb on detrital zircons), and thus to obtain more accurate quantitative provenance estimates from which more robust sediment yields and erosion rates can be calculated.

2. The Marsyandi Basin

The Marsyandi (~ 170 km long; basin area ~ 4750 km^2) is one of the major branches of the Narayani/Sapt Gandaki, in turn one of the major Himalayan tributaries of the River Ganga (Fig. 1). Sourced in Tethys Himalayan sedimentary rocks north of the Annapurna massif (8091 m a.s.l.), it carves steep-walled gorges across Greater Himalayan crystalline rocks southwest of Manaslu peak (8125 m a.s.l.), and finally flows in a broader valley across Lesser Himalayan metasediments, characterized by much lower relief and gentler hillslopes, to eventually join the Trisuli River at Tribeni Ghat (218 m a.s.l.).

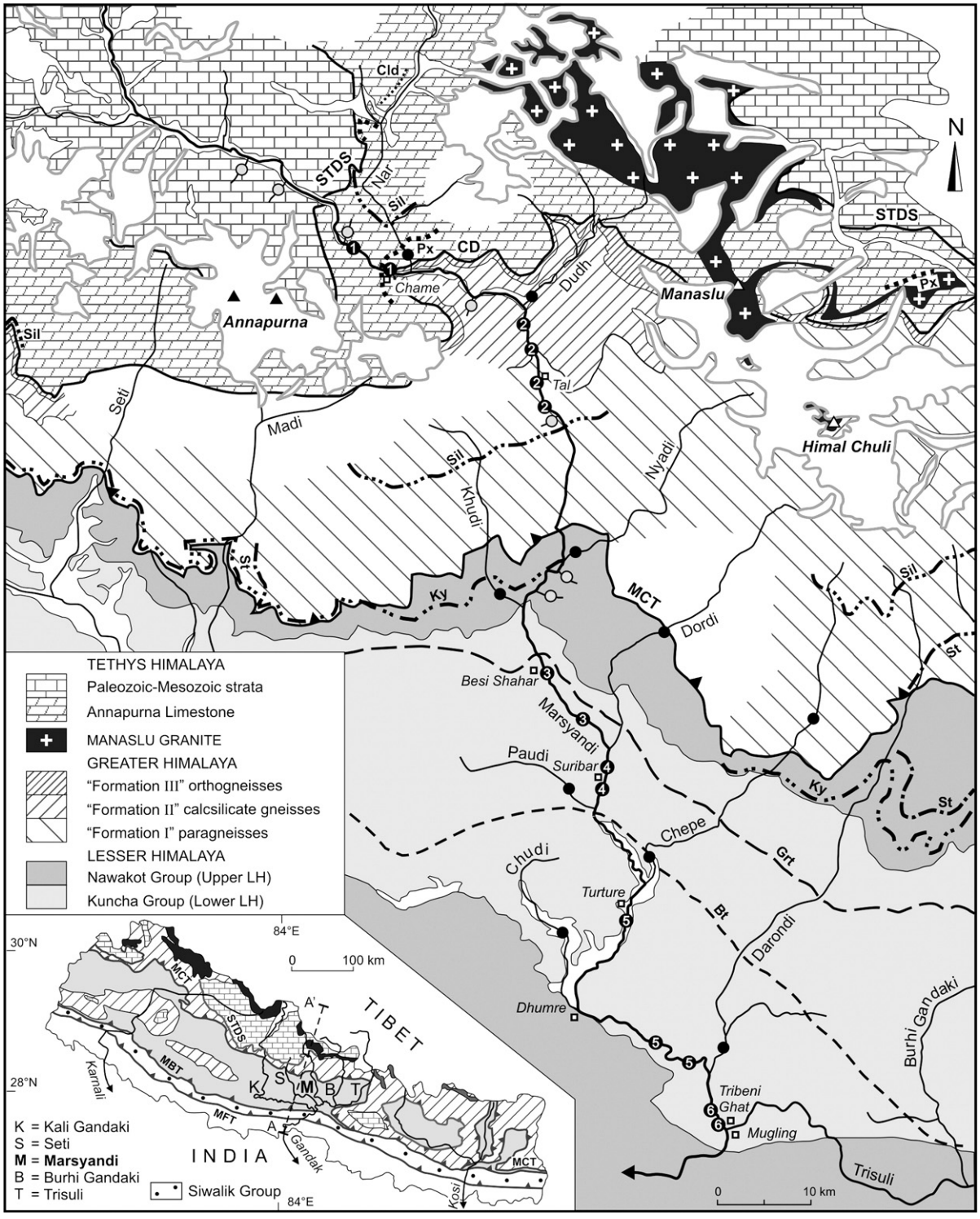

Fig. 1. Geological sketch map of the Marsyandi basin [37]. Isograds (mineral abbreviations as in Fig. 4) and sampled rivers are indicated (numbered dots = trunk river; black dots = major tributaries; grey dots = small tributaries). STDS = South Tibetan Detachment System (Phu Detachment); CD = Chame Detachment; MCT = Main Central Thrust; MBT = Main Boundary Thrust; MFT = Main Frontal Thrust. Geology of Nepal and location of cross-section (AA′) illustrated in Fig. 7 are shown in inset.

Precipitation in the Nepal Himalaya is markedly concentrated during the summer monsoon season (80–98% between May and October), when a low-pressure cell forms on the Tibetan Plateau and humid air masses generated in the Bay of Bengal move counterclockwise toward the northwest and deliver heavy rainfall when colliding with the southern Himalayan front [17]. Because of the major orographic barrier represented by the Greater Himalaya, striking rainfall variations occur perpendicular to the range. Precipitation averages 1.6 m/a in the Lesser Himalaya, but abruptly increases as the monsoon impinges on the southern Greater Himalaya slopes, where maximum rainfall occurs at ~ 3000 m elevation (up to 5 m/a [14,18,25]). Farther north at higher altitudes precipitation decreases rapidly to <2 m/a in the Greater Himalaya and to <0.5 m/a in the dry Tethys Himalaya [16,18,19], where extensive moisture penetration along major river valleys only occurs during exceptional monsoon years. Such a strong topographic control on precipitation distribution can profoundly affect river discharge, erosional processes, and sediment fluxes [36].

2.1. Geological outline

Extensively exposed in the Marsyandi basin are all three major Himalayan tectonic units: a) the Tethys Himalayan sedimentary succession, delimited at the base by the South Tibetan Detachment System; b) the Greater Himalayan amphibolite-facies gneisses, delimited at the base by the Main Central Thrust; and, c) the lower-grade metasediments of the Lesser Himalaya, delimited at the base by the Main Boundary Thrust [37,38]).

The Tethys Himalayan succession includes thick carbonates, overlain by Ordovician quartzites and calcschists, Silurian graptolite-bearing slates, Devonian carbonates and mudrocks, Carboniferous-Permian calcarenites, quartzose sandstones and shales, and finally by mostly carbonate Triassic–Jurassic strata exposed along the watershed [39]. Himalayan deformation and metamorphism decreases upward from amphibolite-facies in the Annapurna marbles, possibly representing equivalents of ?Cambrian Tethyan carbonates comprised between the Chame Detachment at the base and the Phu Detachment at the top [38,40], to anchizonal conditions in Mesozoic strata [41].

The Greater Himalaya is a metamorphic stack including, from base to top [37]: i) paragneisses increasing eastward in thickness from ~ 2 km to >10 km ("Formation I"); ii) ~ 3 km-thick gneisses with calcsilicate minerals (diopsidic/salitic clinopyroxene, blue-green amphibole locally destabilized into biotite, epidote, titanite; "Formation II"), and; iii) ~ 300 m-thick orthogneisses representing metamorphosed Lower Paleozoic granites ("Formation III"). Metamorphic grade increases upward, from kyanite-rich micaschists with zoned epidote above the MCT to metapelites/metapsammites with fibrolitic sillimanite in the upper part of "Formation I", where calcsilicate layers become more abundant. Migmatitic zones rich in K-feldspar increase upward, and finally the Miocene Manaslu leucogranite is found at the top of the Greater Himalaya (23–19 Ma [42]).

The Lesser Himalaya consists of mostly unfossiliferous metasediments exposed in a broad anticlinorium, with much stronger deformation in the northern limb where Tertiary metamorphism reaches lower amphibolite facies (kyanite zone) [37]. The stratigraphically lower part, exposed in the lower Marsyandi basin, consists of very-low to low grade quartzites and phyllites (Kuncha Group), with local metarhyolites, metagranitoids or alkaline metasyenites. The upper part includes commonly dolomitic metacarbonates alternating with schists and quartzites (Nawakot Group). Amphibolites occur in both Groups [37].

3. Bulk petrography and heavy minerals

Thirty-six, mostly fine- to medium-grained sand samples were collected on active bars of the Marsyandi River and its major tributaries during several field campaigns from 1993 to 2005. Bedload samples from minor tributaries draining specific source areas were also studied to identify the signatures of each structural domain ("first-order sampling scale" of [43]). In each sample, 400 points were counted by the Gazzi–Dickinson method in thin section [44] and 200–250 transparent heavy minerals were counted on grain mounts [complete database provided in Appendices A1 and A2.

A detailed classification scheme allowed us to collect quantitative information on metamorphic rank of rock fragments (MI index [45]). Thin sections were stained with alizarine red to distinguish calcite from dolomite. Heavy minerals were separated in sodium metatungstate (density 2.9 g/cm^3), using the 63–250 μm fraction treated with acetic acid and sodium ditionite.

3.1. Sands from distinct geological domains

Streams draining Tethys Himalayan strata carry abundant sedimentary (limestone, shale, dolostone) and very-low-grade metasedimentary (slate, phyllite, metacarbonate) grains, with minor quartz and rare feldspars (Fig. 2A). Heavy minerals include a few recycled ultrastable grains (zircon, tourmaline, rutile) and low-

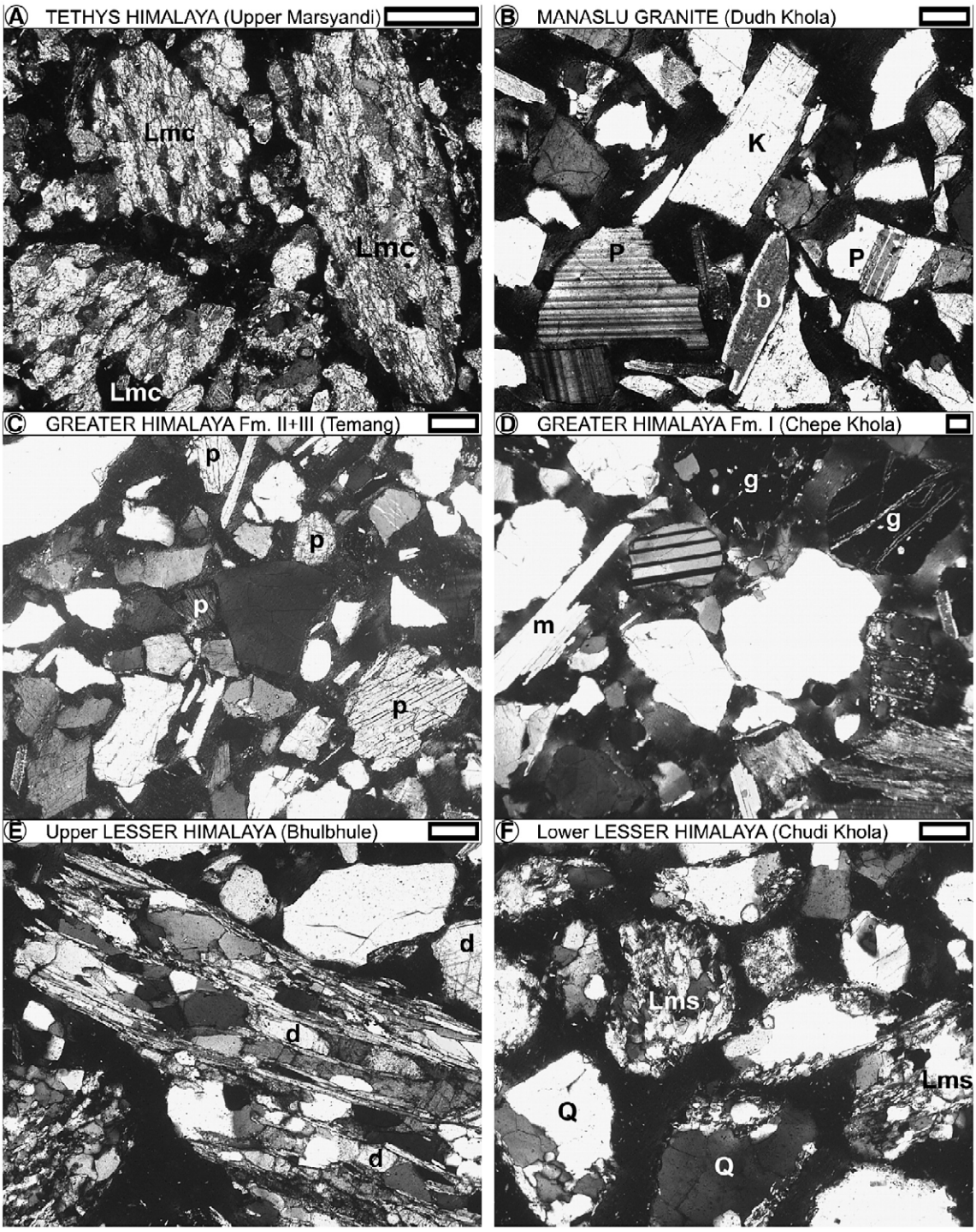

Fig. 2. Compositional end-members in the Marsyandi basin. A) Low-rank metasedimentary detritus rich in metacarbonate grains (Lmc); B) granitic detritus rich in feldspars (P=plagioclase; K=K-feldspar; b=biotite); C) very-high-rank gneissic detritus rich in clinopyroxene (p); D) very-high-rank gneissic detritus rich in garnet (g) and micas (m=muscovite); E) high-rank metasedimentary detritus rich in metapsammite and metadolostone (d=dolomite) grains; F) medium-rank metasedimentary detritus rich in quartz (Q) and metapsammite (Lms) grains. Scale bars =125 μm; all photos with crossed polars.

grade metamorphic species from pre-Carboniferous units (purplish epidote, chloritoid). Calcareous sparite grains dominate detritus from the Annapurna marbles, which also yield titanite, amphibole, and clinopyroxene.

Quartzofeldspathic sands of tributaries draining Greater Himalayan gneisses contain abundant biotite and muscovite. The rich heavy-mineral assemblages are either dominated by clinopyroxene associated with titanite and blue-green amphibole from "Formation II" calcsilicate gneisses (Fig. 2C), or by garnet associated with kyanite or fibrolitic sillimanite from "Formation I" paragneisses (Fig. 2D). K-feldspars are supplied in abundance by the Manaslu Granite and "Formation III" orthogneisses (Fig. 2B).

Minor tributaries draining lower-amphibolite-facies metasediments of the Nawakot Group carry quartz, micas, high-rank metapelite/metapsammite and metacarbonate (mostly dolomite) grains, and minor feldspars (Fig. 2E). Heavy minerals include epidote (commonly zoned with zoisite core and clinozoisite rim), kyanite, blue-green amphiboles, etched clinopyroxenes, tourmaline, rutile, garnet, staurolite and apatite. The Paudi and Chudi Kholas, draining upper greenschist-facies Kuncha Group metasediments, carry dominant quartz and medium-rank (Chudi Khola) to medium/high-rank (Paudi Khola) metapsammite and metapelite grains, with minor feldspars and micas (Fig. 2F). Heavy minerals include blue-green amphiboles, tourmaline, and epidote.

3.2. Sands of the trunk river and major tributaries

Composition of Marsyandi sands changes progressively as the river cuts downstream across the Himalayan belt (Fig. 3). Upstream of the Chame Detachment, sedimentary/metasedimentary detritus is derived entirely from Tethys Himalayan units. Feldspars increase sharply downstream of the confluence with the Dudh Khola, draining the Manaslu Leucogranite and "Formation III" orthogneisses. Quartz, feldspars and metamorphic rank of lithic grains markedly increase across the Greater Himalaya, as well as heavy mineral concentrations. The Dordi and Nyadi Kholas mainly supply clinopyroxene, garnet and sillimanite, the Khudi Khola kyanite and clinopyroxene, the Chepe and Darondi Kholas garnet and kyanite. Across lower-altitude lower reaches, where Lesser Himalayan metasediments are exposed, quartz and micas increase with respect to feldspars and heavy minerals, and metamorphic rank of lithic grains progressively decreases. The final composition of Marsyandi sands includes clinopyroxene–garnet–kyanite heavy-mineral assemblages and significant feldspars, indicating prominent contribution from the Greater Himalaya.

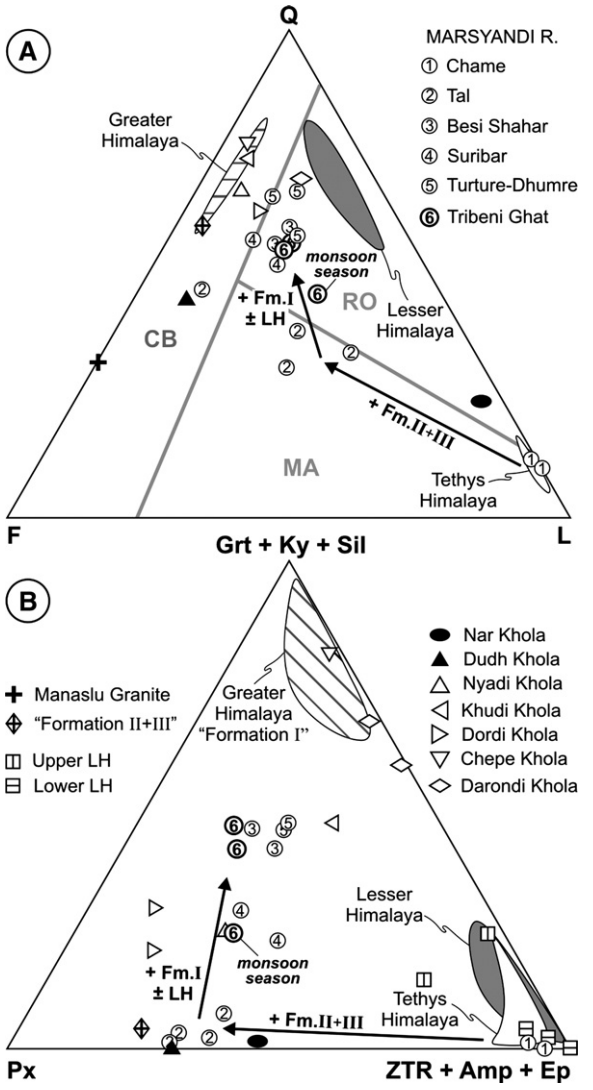

Fig. 3. Composition of Marsyandi sands. A) Bulk petrography (RO="Recycled Orogen"; CB="Continental Block"; MA="Magmatic Arc" provenance fields after [65]). B) Heavy minerals. Abundant limestone grains and pyroxene in the final Marsyandi sample collected in July document greater contributions from the upper catchment (Tethys Himalaya and "Formation II" calcsilicate gneisses) during the monsoon. 95% confidence regions about the mean calculated after [66]. Parameters as in Fig. 4. Because low-density granitic rocks supply negligible heavy minerals [46,60], the heavy-mineral mode for the Manaslu Granite is not included.

3.3. Concentration of heavy minerals and micas

Heavy minerals are powerful provenance indicators, that allow discrimination of distinct source rocks even within the same tectonic unit (e.g., "Formation II" calcsilicate gneisses yielding clinopyroxene versus "Formation I" paragneisses supplying garnet and kyanite or fibrolitic sillimanite). Heavy-mineral concentration by

itself is diagnostic of distinct provenances [46]. Because of their anomalous density or shape, however, accessory minerals such as ultradense zircons or platy micas behave differently and easily segregate from main framework grains in the depositional environment. A uniform distribution of the investigated mineral, either in rocks exposed across the catchment or in river sediments, cannot be assumed when provenance and erosion rates are inferred from geochronological data on zircon, apatite or micas [33,34]. The average abundances and standard deviations of accessory minerals used in detrital geochronology, as observed in Marsyandi sands and in detritus from each geological domain, are given in Fig. 4.

4. Quantifying provenance

Terrigenous fluvial sediments are complex mixtures of monocrystalline and polycrystalline grains eroded from diverse geological units, and supplied in various proportions by numerous streams to successive segments of a trunk river. If end-member compositional signatures of detritus derived from each main geological unit and carried by each main tributary are known, relative contributions from each of these sources to total sediment load can be quantified mathematically with forward mixing models [47]. This method allows us to partition the total sediment flux, and thus to obtain independent estimates of sediment yield and erosion rates from distinct subcatchments [33,48,49].

4.1. The Marsyandi laboratory

Because of logistical accessibility and geological information with no equivalent in other Himalayan regions, the Marsyandi basin represents an excellent natural laboratory in which to test the potentialities and limitations of quantitative provenance analysis. The river drains exclusively upstream of the Main Boundary Thrust, and its sands are therefore chiefly first-cycle and free from detritus recycled from the Siwalik molasse, which represents a major problem in provenance analysis of foreland-basin deposits.

Marsyandi sands were collected in six successive sites along the trunk river (Fig. 4), upstream of major geological boundaries and/or downstream of major confluences. In order to minimize various sources of error, duplicate samples were collected in each of the six sites during different field seasons, by different operators, and in different localities. This sampling scheme enables us to accurately constrain relative contributions from each major tributary, as well as from each geological unit, by performing integrated calculations which simultaneously satisfy best-fit criteria for five successive tracts of the river [method described in Appendix A4].

In order to test for both intra-sample and inter-sample compositional variability related to grain size, hydraulic-sorting and seasonal changes, the two final Marsyandi samples were analysed separately for each grain-size subclass at 0.5Φ intervals for both bulk petrography and heavy minerals.

4.2. The calculation of relative sediment budgets

Relative contributions from various detrital sources, although assessed from an integrated petrographic-mineralogical data-set of up to fifty compositional parameters, are non-unique and uncertain, and suffer from intrinsic variability of complex natural phenomena. In mountain catchments, composition of river sands is influenced by seasonal variations in relative sediment discharge, different grain-size distributions of tributary and trunk-river sediments, imperfect mixing, and local effects created by large landslides or alluvial-fan growth at confluences. Accelerated reworking of Quaternary terraces (assessed at ~ 2–3% of Marsyandi load [26]) may lead to anomalous sediment fluxes and overestimated rates of bedrock erosion.

The results obtained were tested for internal consistency by performing several repeated sets of independent calculations for the integrated petrographical–mineralogical data-set or separately for bulk petrography and heavy minerals, and by following alternative geologically-plausible criteria and different weighting strategies

Fig. 4. Sediment yields and erosion rates as inferred from detrital modes and heavy mineral assemblages of Marsyandi sands. A major source of uncertainty is the compositional change observed at Tribeni Ghat between the monsoon and post-monsoon season. Error in assessing total Marsyandi load significantly influences all absolute values, but without altering erosion patterns. Estimated areas and average rock densities are given for each subcatchment. Q=quartz; F=feldspars; L=lithic grains (Lc=carbonate; Lsm=other sedimentary and low-rank metasedimentary; Lm=medium- to high-rank metamorphic). ZTR=zircon+tourmaline+rutile; Ep=epidote-group minerals; Grt=garnet; Ky=kyanite; Sil=sillimanite; Amp=amphiboles; Px=pyroxenes; Tit=titanite; Ap=apatite; &=others. Rank of metamorphic grains (MI index [45]), heavy-mineral concentration (HMC index [46]), and abundance of micas (Ms=muscovite; Bt=biotite), zircon (Zrn) and apatite (Ap) with respect to bulk sediment are also given. Strong dependence of relative and absolute abundances of accessory grains on both provenance and hydraulic processes must be taken into full account when geochronological or geochemical data on single mineral species are used to infer provenance and sediment budgets.

[49]. The standard deviation of the results obtained with this trial-and-error approach is believed to provide an empirical estimate of the uncertainty associated with the average values.

It must be kept in mind that results based on bedload sands may not be applicable to the mud fraction carried in suspension (~ 60% of total Marsyandi load [21,26]). Also, quantitative provenance analysis may be biased by

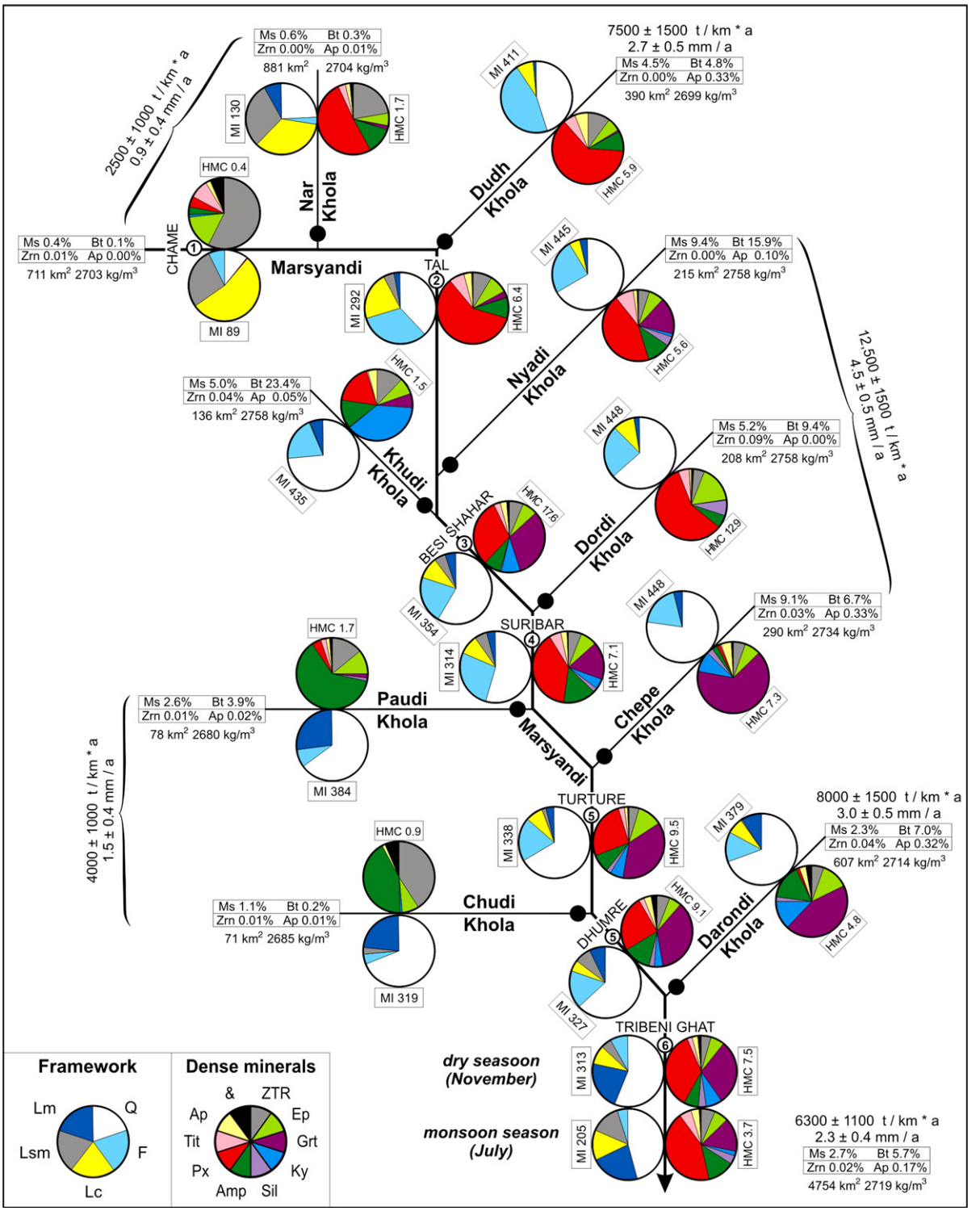

selective physical or chemical destruction of non-durable and unstable grains, seasonal changes in sediment transport, and hydraulic segregation of grains with different size, density and shape [50,51].

4.3. Uncertainties caused by destruction of unstable grains

Because of limited storage times and rapid transport from source to basin [20], and because physical comminution is held to have little effect on detrital modes [52], sediment composition in high-relief mountain catchments is generally assumed to faithfully reflect the mineralogy of parent rocks even in monsoonal climates [53].

In order to verify the incidence of chemical weathering, we quantitatively analysed dissolution features shown by detrital grains with different chemical stabilities [54]. The large majority of heavy minerals throughout the Marsyandi catchment are fresh or only slightly altered. Only 9±4% of detrital pyroxenes and 3±2% of detrital amphiboles are etched, a comparable amount show incipient corrosion, and very few (mostly pyroxene) show skeletal features indicative of extensive dissolution. An exception is represented by small tributaries draining "Formation I" or the Nawakot Group in the middle Marsyandi valley, which contain a few deeply etched clinopyroxene grains probably derived from altered Quaternary terraces. Epidote, staurolite, garnet, titanite, or apatite occasionaly show incipient corrosion, but never extensive dissolution features. Selective destruction of unstable silicate grains (including plagioclase) can thus be considered negligible.

Experimental results on Marsyandi gravel bedload showed that abrasion rates may vary by up to two orders of magnitude for various pebble lithologies (lowest for quartzite, low for granite and "Fm. II" calcsilicate gneiss, intermediate for "Fm. I" paragneiss, marble and Kuncha metasandstone, high for sandstone and schist), and selective destruction of non-durable lithologies is suggested by downstream decrease of sandstone, limestone and schist, with parallel increase of gneiss and quartzite [26]. These effects, however, are difficult to separate from downstream dilution by supply from tributaries and hillslopes, and cannot be directly extrapolated to sand-sized detritus. The type and amount of sand grains produced (by abrasion of gravel) and destroyed (ground into mud) during sediment transport remain unconstrained.

If partial destruction of soluble carbonate or non-durable shale/slate grains (representing 53±6% and 27±14% of Tethys Himalaya-derived detritus, respectively) takes places during transport, the Tethys Himalayan contribution would be underestimated. Decrease of Tethys Himalayan-derived unstable grains, however, is seen to abruptly take place immediately downstream of the Dudh Khola confluence, chiefly reflecting rapid dilution, and again across the middle part of the basin, chiefly reflecting dilution from "Formation I"-derived carbonate-free gneissic detritus. In lower reaches, the dolomite/calcite ratio increases because dolostone grains are supplied by the Nawakot Group, whereas limestone grains continue to decrease, again reflecting dilution rather than dissolution [21].

Our calculations do not show a systematic deficiency in calcareous grains in lower Marsyandi reaches, we failed to obtain improved fits by modeling various degrees of carbonate dissolution, and our results do not change significantly if carbonate and shale/slate grains are neglected (and other parameters recalculated to 100%), suggesting that selective destruction of unstable grains does not represent a major source of error. In fact, dissolution of carbonate grains is unlikely to take place during fluvial transport because Marsyandi waters are saturated with respect to calcite [21]. Chemistry of river waters nevertheless indicates that carbonate dissolution is an extensive process [22–24], and that erosion rates for carbonate-rich units (e.g. Tethys Himalaya) are slightly underestimated if chemical erosion is not taken into account (~ 0.05 mm/a for the Marsyandi catchment [21]). Chemical erosion is held to be an order of magnitude less for silicate rocks (~ 0.005 mm/a for the Marsyandi catchment [21]), and thus negligible.

4.4. Uncertainties caused by grain size and sorting

Significant uncertainties in provenance calculations are potentially caused by grain-size fractionation and hydraulic processes, such as concentration of heavy minerals in placer deposits or of platy micas in low-energy subenvironments [54]. In Marsyandi samples, strong hydraulic control is indicated locally by nearly one-order-of-magnitude variability in the mica/heavy-mineral ratio, and by heavy-mineral concentrations richer than any upper-crustal source rock can yield [46].

The two final Marsyandi samples, analysed separately at 0.5Φ intervals, display intra-sample compositional variability associated with grain density and shape [55]. Heavy minerals are concentrated in the fine tail, whereas relative abundances of platy micas and fibrous sillimanite increase in the coarse tail. Although partly related to grain-size and hydraulic-sorting effects (e.g., Greater Himalayan contributions would be overestimated for placer deposits, the Greater Himalaya being the dominant source of heavy minerals), inter-sample variability is principally ascribed to seasonal changes in sediment transport.

4.5. Uncertainties caused by seasonal changes

Because most studied samples were collected in November, our data-set is not comprehensive enough to test systematically for seasonal changes of sand composition throughout the Marsyandi catchment. We thus designed a single accurate test for the Marsyandi basin overall, and minimized grain size differences by comparing homologous 0.5Φ subclasses of the two samples collected at Tribeni Ghat in July 2005 (full monsoon) and November 2000 (post-monsoon season).

In the finer-grained July sample (2.7Φ), significantly higher limestone and shale/slate grains, more K-feldspar, clinopyroxene, titanite, ultrastable heavy minerals, and chloritoid consistently suggest greater contributions from Tethys Himalaya to upper Greater Himalaya metasediments and granites exposed in the upper catchment. In the coarser November sample (1.7Φ), conversely, higher quartz and dolostone grains, more garnet and kyanite suggest higher contributions from greenschist-facies to amphibolite-facies metasediments of the lower catchment ("Formation I" to Lesser Himalaya).

Greater contribution from calcareous rocks of the upper catchment during the monsoon is independently suggested by geochemical data on suspended load collected in July in the middle to lower Marsyandi Valley, which consistently shows nearly double calcite content with respect to bedload collected in the same sites after the monsoon in November (Fig. 5). Because the bulk of sediment transport takes place during the monsoon season, calculations from our data-set may underestimate erosion in the upper catchment (Tethys Himalaya and upper Greater Himalaya).

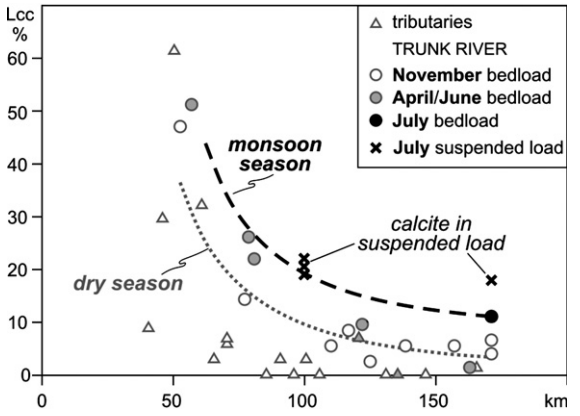

Fig. 5. Seasonal variability in composition of Marsyandi sands. Bar sands collected during the monsoon season (July; black dashed line), or even during the first heavy pre-monsoon rains (April/June), tend to be richer in limestone grains (Lcc) than post-monsoon bar sands (November; grey dotted line). Greater contributions from the Tethys Himalaya during the monsoon is independently suggested by geochemical data on suspended load sediments collected in July in the middle (samples kindly provided by D. Burbank) to lower Marsyandi valley.

5. Quantifying sediment yields and erosion rates

The calculation of sediment yields and erosion rates from provenance estimates is affected primarily by large uncertainties in the assessment of sediment fluxes, and subordinately by imperfect knowledge of outcrop areas and rock densities [48]. If information on suspended river loads is typically scarce and inconsistent, bedload data are generally lacking altogether. The bedload is thus commonly assumed arbitrarily as ~ 10% of the total load [56], even though this value is suspected to reach as high as 60% for Himalayan rivers [21].

5.1. Uncertainties in assessing total Marsyandi load

Although a dam is being built in the middle catchment upstream of the Dordi Khola, the Marsyandi River was unregulated when the studied samples were collected. In order to estimate reservoir lifetime, sediment fluxes have been monitored at the dam site since 1990. Suspended sediment concentration increases in June at the beginning of the monsoon season, and reaches up to 10,000–15,000 ppm between July and September. Annual suspended load is calculated at 18.8 10^6 t/a [57], and bedload is estimated to represent ~ 17% of total load (22–25% according to [26]). Total load is thus estimated at 22.5 10^6 t/a, which for a basin area of 2729 km^2 corresponds to an average sediment yield of 8250 t/km^2 a and an erosion rate of 3.0 mm/a. The total Marsyandi flux, which includes detritus produced in lower reaches and contributed by the Dordi, Chepe, and Darondi Kholas, was evaluated at $\geq$31 10^6 t/a, equivalent to an average erosion rate of 2.4 mm/a [21].

Among tributaries, sediment load was assessed at 1.4 10^6 t/a for the Khudi Khola (136 km^2), corresponding to an average yield of ~ 10,200 t/km^2 a and erosion rate of 3.7 mm/a [29]).

For the whole Narayani/Gandak basin (~ 31,000 km^2), total load was estimated — from suspended-load measurements and assuming that bedload represents ~ 13% of total load (12–18% [26]) — at 121 10^6 t/a [58]. This corresponds to an average sediment yield of ~ 3900 t/km^2 a and an erosion rate of 1.4 mm/a. Average suspended loads of 82 10^6 t/a [59], and total loads between 109 [13] and $\geq$160 10^6 t/a [21], were also estimated.

Sediment yields may have been enhanced during latest decades by human activities and deforestation, particularly in intensively cultivated areas at altitudes

below 2000 m a.s.l. [18,57]. Based on available information [21,57], we assume here a total Marsyandi sediment load of 30±5 10^6 t/a (corresponding to an average erosion rate of 2.3±0.4 mm/a). This assumption markedly influences the absolute values of sediment yields and erosion for each Marsyandi subcatchment given in the following paragraphs, but it does not alter erosion patterns.

5.2. Uncertainties in assessing outcrop areas

Beside problems caused by different projections of topographic or geological maps, or by local ambiguities in the definition of drainage divides, discrepancies may result from different geological interpretations [34]. We chose to adhere here to the 1:200,000 geological map by Colchen et al. [37], which is based on extensive fieldwork, supplemented by exhaustive lithological descriptions, and far more detailed than maps available for most other Himalayan regions. In recent years, distinct tectonic boundaries were identified at the top of the Greater Himalayan nappe stack (Phu and Chame Detachments [38]). The outcrop area between these two detachments largely consists of Annapurna marbles, which we chose to consider jointly with Tethys Himalaya sedimentary units principally because these higher-grade metamorphic rocks also supply detritus dominated by carbonate rock fragments.

A thornier problem is revealed by pyroxene-rich sands carried by major tributaries in the middle Marsyandi basin (Dordi and Nyadi Kholas). This indicates a much more significant contribution from "Formation II"-type calcsilicate gneisses than indicated by the only sporadic exposures of such rocks displayed along the southwestern flank of the Himal Chuli [37]. More detailed geological information on this area would help us greatly to more precisely assess erosion rates across the Greater Himalaya.

Outcrop areas for each subcatchment and tectonic unit are given in Figs. 4 and 6.

5.3. Uncertainties in assessing rock densities

The average density of each major geological unit exposed in the catchment can be assessed not only by sporadic data in the literature [20] but also directly from the integrated petrographical–mineralogical composition of detritus derived entirely from each single unit (SRD index [46]). In spite of local hydraulic-sorting effects, errors turn out to be ≤1% for most non-porous metamorphic and plutonic source rocks [60]. Uncertainties in assessing rock densities in the Marsyandi basin are therefore small, and only cause minor errors in the conversion of sediment yields into erosion rates. Rock densities for each subcatchment and tectonic unit are given in Figs. 4 and 6.

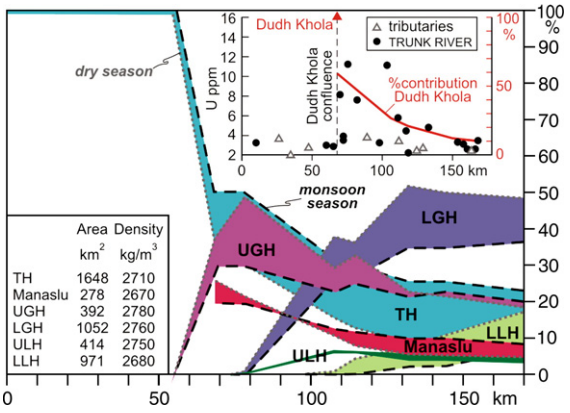

Fig. 6. Estimated contributions from distinct geological units to the total Marsyandi load. Relative supply from the Tethys Himalaya is estimated to be greater during the monsoon season (black dashed lines), whereas supply from the lower Greater Himalaya is prominent in the dry season (grey dotted lines). Inset shows limited contribution from the Manaslu Granite exposed at extreme elevations in the Dudh Khola catchment, as documented by rapid dilution of U content in trunk river sediments (bulk-sediment U concentrations measured at SARM-CNRS Nancy by ICP-MS [complete data-set provided in Appendix A3]). Areas and average rock densities are given for each tectonic unit. TH=Tethys Himalaya; UGH=upper Greater Himalaya ("Formation II+III"); LGH=lower Greater Himalaya ("Formation I"); ULH=upper Lesser Himalaya (Nawakot Group); LLH=lower Lesser Himalaya (Kuncha Group).

6. Sediment budgets

Estimates reported here are obtained by considering the complete sample set. The largest uncertainty is associated with seasonal and/or grain-size changes in sediment composition. Maximum contributions from the Tethys Himalaya and upper Greater Himalaya, or from the lower Greater Himalaya and Lesser Himalaya, are calculated if true composition of Marsyandi load corresponds to our finer-grained monsoon sample, or to our coarser-grained post-monsoon sample, respectively (Fig. 6).

6.1. Relative contributions from distinct subcatchments

Our calculations indicate that 29±12% of the Marsyandi load is produced in the upper half of the catchment (Tethys Himalaya and upper Greater Himalaya). The Dudh Khola, draining the Manaslu Granite and upper Greater Himalaya units, contributes more sediment than the upper Marsyandi and Nar Khola, draining a much wider area within the Tethys Himalaya (Fig. 4). The

tributaries of the middle Marsyandi basin (Nyadi, Khudi, Dordi, Chepe Kholas), draining largely "Formation I" and subordinately the Lesser Himalaya, contribute 54±10% of total Marsyandi flux. The remaining 17±4% is supplied in the lower part of the catchment by the Darondi Khola and minor tributaries draining Lesser Himalayan units (Paudi, Chudi Kholas).

Sediment yields and erosion rates are thus much lower in the upper Marsyandi and Nar Khola catchments than in the Dudh Khola catchment (Fig. 4). Maximum yields are assessed for the Nyadi, Khudi, Dordi and Chepe basins, whereas lower erosion values characterize the Darondi basin and rivers draining only the Lesser Himalaya.

6.2. Sediment yields and erosion rates for distinct geological domains

Several series of independent calculations from our integrated petrographic-mineralogical data-set indicate that Tethys Himalayan units (including Annapurna metacarbonates) provide 13±5% of the Marsyandi bedload, Greater Himalayan units 68±3% (6±2% from Manaslu Granite; 12±2% from "Formations II+III"; 49±4% from "Formation I") and Lesser Himalayan units 20±2% (6±1% from the Nawakot Group and 14±3% from the Kuncha Group) (Fig. 6). Relative contributions from each geological domain were assessed both directly by end-member calculations for the total Marsyandi basin, or indirectly by partitioning the estimated flux of each major tributary. This was done both according to end-member calculations or proportionally to areal exposures within each catchment. In the Nyadi and Dordi basins, all Greater Himalaya-derived detritus has been ascribed to "Formation I" as indicated in the map [37], even though sand composition proves that "Formation II"-type calsilicate gneisses are extensively eroded along the southwestern flank of the Himal Chuli. Otherwise, we would have been forced to assign an arbitrary area to "Formation II" in the Nyadi and Dordi catchments, in order not to overestimate erosion rates for this unit.

The contribution from the Manaslu Granite was calculated by assuming that, in such rapidly eroded mountain areas of extreme relief and arid climate, granite-derived detritus maintains the same composition as the parent rock (quartz 32%, plagioclase 37%, K-feldspar 21%, muscovite 7%, biotite 3% [37]). With such end-member mode, composition of Dudh Khola sand indicates that almost half of it originates from the granite and the remaining half from "Formation II" calsilicate gneisses, with minor contribution from the Annapurna marbles.

Partitioning of a Marsyandi sediment flux of 30±5 10^6 t/a according to these provenance estimates (and to drained areas and rock densities given in Fig. 6) implies sediment yields of 2500±1300 t/km^2 and erosion rates of 0.9±0.5 mm/a for Tethys Himalayan units, 11,600±2800 t/km^2 a and 4.2±1.0 mm/a for the Greater Himalaya (6300±2500 t/km^2 and 2.4±0.9 mm/a for the Manaslu Granite; 8700±3000 t/km^2 and 3.1±1.1 mm/a for "Formations II+III"; 14100±3400 t/km^2 and 5.1±1.2 mm/a for "Formation I"), and 4300±1500 t/km^2 and 1.6±0.6 mm/a for the Lesser Himalaya (4600±1600 t/km^2 and 1.7±0.6 mm/a for the Nawakot Group; 4100±1800 t/km^2 and 1.5±0.7 mm/a for the Kuncha Group).

6.3. Discrepancies with estimates obtained by different methods

Our calculations suggest that the Greater Himalaya is eroding much faster than the Tethys and Lesser Himalaya, at rates that compare well with previous estimates (=2–5 mm/a [13,14,29]). We infer that sediment yields decrease northward, although zircon and apatite fission-track data failed to document erosion gradients across the Greater Himalaya [14,19,28]. This discrepancy may be ascribed to different scales of observation, because our data reflect short-term erosion, whereas apatite fission-tracks record erosion at the >100,000 a scale [14]. Alternatively, erosion patterns across the Greater Himalaya may be more homogeneous than we calculated. Composition of the fine-grained final Marsyandi July sample suggests in fact that rapid erosion of the upper catchment may take place when large storms penetrate far north during the peak of the summer monsoon. Moreover, we did not consider the mud fraction carried in suspension, where detritus from the upper catchment may be concentrated as a result of longer high-energy transport across steep mountain reaches.

Our estimates are markedly higher than long-term, catchment-averaged estimates deduced by modelling of detrital muscovite ^{40}Ar/^{39}Ar data (=1 mm/a for Dudh and Nyadi catchments [32]; ~ 2 mm/a for Nyadi, Khudi, Dordi, Chepe and Darondi catchments [33]). The discrepancy may stem again from different time-scales of observation [27], or from faulty assumptions underlying the usage of detrital muscovite ^{40}Ar/^{39}Ar data as a proxy for erosion rates [61].

Our results are in disagreement also with Amidon et al. [34,35]. By dating detrital zircon in Marsyandi sands, they observed that Greater Himalayan units provide 4 to 8 times more zircon grains than Lesser Himalayan units but, after correcting for different concentrations of zircon

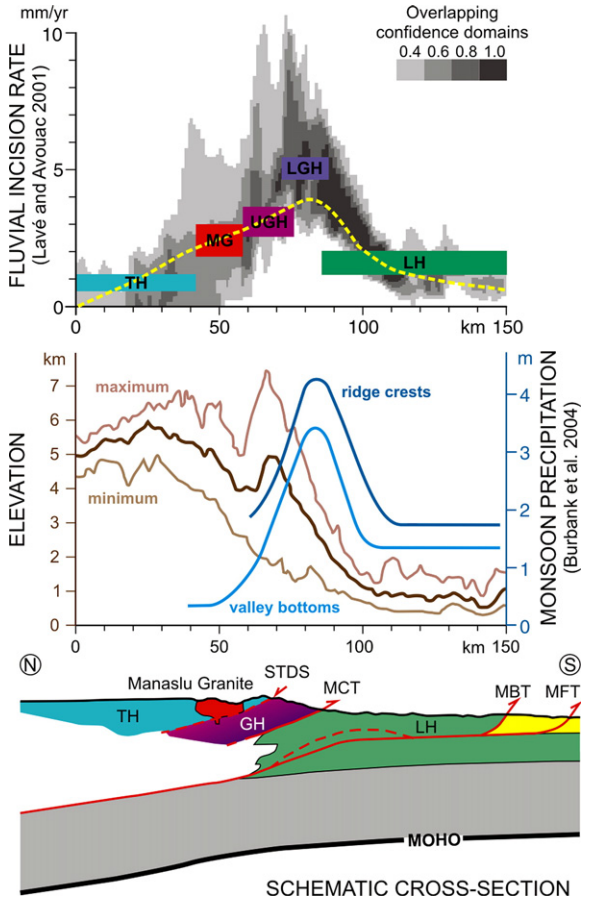

Fig. 7. Relationships between geology, topography, climate, and erosion in the Nepal Himalaya. Erosion rates calculated from our dataset (colour boxes in upper panel: TH=Tethys Himalaya; MG=Manaslu Granite; UGH=upper Greater Himalaya; LGH=lower Greater Himalaya; LH=Lesser Himalaya) are highest in the lower Greater Himalaya, where rainfall is most intense, and decrease progressively northward towards arid Tibet in spite of extreme topographic elevation and relief. Our estimates compare remarkably well with incision rates deduced from shear-stress calculations along major Central Nepal rivers (Kali Gandaki to Sun Kosi [13]; confidence domains shown by grey shades), and with mean landscape denudation calculated by numerical model of [64] (shown by dashed yellow line). Data projected along a N18°E profile (see inset of Fig. 1 for location), orthogonally to main Himalayan structures.

in Greater and Lesser Himalayan detritus, sediment yield and erosion rates resulted to be ~ 3 times more in the northernmost Lesser Himalaya than in the Greater Himalaya [34,35]. Although our data confirm that Greater Himalayan units shed more zircon than Lesser Himalayan units (Fig. 4), errors may be easily introduced by overcorrection, because the concentration of ultradense zircon grains may vary locally by an order of magnitude or more because of hydraulic-sorting and grain-size effects.

6.4. Erosion patterns across the Himalayan belt

Our calculations suggest that the tectonically-lower "Formation I", exposed at lower altitudes along monsoon-drenched southern slopes, is eroding faster than the structurally-higher "Formations II+III", exposed at higher altitudes and in drier climatic conditions to the north (Fig. 7). Erosion rates decrease further for the Manaslu Granite, which occupies the extreme-altitude and highly-glaciated northern half of the catchment but contributes less detritus to the Dudh Khola than "Formation II" gneisses exposed less widely to the south. Minimum rates are reached for the Tethys Himalaya, exposed at 4000–6000 m a.s.l. in the arid north.

Spatial correlation with precipitation gradients suggests that climate exerts a strong control over erosion rates across the Nepal Himalaya [30]. Focused erosion may be driven by tectonic uplift of the MCT hangingwall related with either out-of-sequence thrusting [10] or passive transport above a mid-crustal ramp [13], which in turn may reflect positive feedback between uplift and monsoonal rainfall [3,11].

Relatively low sediment yields inferred for the high-relief Manaslu region suggest that extreme topography has little effect on erosion in the absence of significant precipitation. Beside lithology (leucogranites, massive metacarbonates), dry climate may represent a key factor to explain the location of Nepalese eight-thousanders, all straddling the boundary between the Tethys and Greater Himalaya at the southern border of the Tibetan rain shadow [19]. Flux of snow and ice is virtually non-existent above 6200–6300 m a.s.l., and hence glacial erosion is inefficient [62]. High peaks (Manaslu, Annapurna, Dhaulagiri) may thus be viewed as topographic anomalies determined by rock strength [63], which surface processes are not intense enough to remove.

7. Conclusions

Sediment composition can be used to define erosion patterns across mountain catchments and subcatchments [49,53]. The Marsyandi basin of Central Nepal, located between two peaks above 8000 m a.s.l. and perhaps the most geologically and geomorphologically-studied of the Himalaya [14], is an excellent area to test the potentialities and limitations of the method.

Specific mineralogical tracers in detritus from the Tethys Himalaya (lithic sands rich in carbonate and low-rank metasedimentary grains), Manaslu Granite (feldspathoquartzose sands), "Formation II" (gneiss sands with clinopyroxene), "Formation I" (gneiss sands with garnet and kyanite or fibrolitic sillimanite), and

Lesser Himalaya (quartzose sands with medium-rank metasedimentary and locally dolostone grains) allowed us to assess relative contributions from each tectonic unit to the Marsyandi load. If the latter is held to be 30 ± 5 10^6 t/a, relative estimates can be easily converted into sediment yields and erosion rates.

Our calculations lend support to focused erosion of the tectonically-lower, southern part of the Greater Himalaya in the hangingwall of the MCT Zone ("Formation I"), where annual rainfall reaches 5 m/a and sediment yields and erosion rates 14100 ± 3400 t/km^2 and 5.1 ± 1.2 mm/a [14,30]. Erosion rates are markedly lower for Lesser Himalayan units to the south, where monsoonal rainfall decreases and relief is low. They progressively decrease also in the upper Greater Himalaya to the north in spite of extreme topography, because precipitation is too scarce to feed significant ice flux and glacial activity [18,62].

Erosion patterns, therefore, are not controlled directly by altitude and relief. Rather, erosion is coupled with peak monsoon rains along the southern front of the Greater Himalaya, suggesting that erosion and precipitation may be spatially associated with active tectonic uplift [10,11], in a feedback loop which is compatible with both "channel-flow type" tectonic extrusion of Greater Himalayan metamorphic rocks [3] and tectonic uplift above a mid-crustal ramp [13,64] (Fig. 7). Thus, our data cannot resolve the elusive "chicken-and-egg" nature of tectonic–climatic coupling [8]: does rainfall promote focused erosion and crustal exhumation, or is orographic precipitation triggered by tectonically-generated topography?

In both cases, the Nepalese eight-thousanders in this region may be viewed as topographic anomalies created by rock strength, active uplift, and limited erosion in cold desert climate at the southern edge of the Tibetan rain shadow.

Acknowledgments

The paper benefited from careful reviews by Ray Ingersoll, Hilmar von Eynatten, and an anonymous reviewer, and from discussions with Laurent Godin, Bruno Lombardo, Yani Najman, Franco Rolfo, and Igor Villa. Two sampling campaigns greatly benefited from logistic support by Tank Ojha and "Himalayan Experience", and from financial support of the National Science Foundation Continental Dynamic Program (grant ERA-99-09647).

Appendix A. Supplementary data

Supplementary data associated with this article can be found, in the online version, at doi:10.1016/j.epsl.2007.04.010.

References

[1] J.P. Avouac, E.B. Burov, Erosion as a driving mechanism of intracontinental mountain growth, J. Geophys. Res. 101 (1996) 17747–17769.
[2] S.D. Willett, Orogeny and orography: the effects of erosion on the structure of mountain belts, J. Geophys. Res., Solid Earth 104 (1999) 28957–28981.
[3] C. Beaumont, R.A. Jamieson, M.H. Nguyen, B. Lee, Himalayan tectonics explained by extrusion of a low-viscosity crustal channel coupled to focused surface denudation, Nature 414 (2001) 738–742.
[4] P.K. Zeitler, A.S. Meltzer, P.O. Koons, D. Craw, B. Hallet, C.P. Chamberlain, W.S.F. Kidd, S.K. Park, L. Seeber, M. Bishop, J. Shroder, Erosion, Himalayan geodynamics, and the geomorphology of metamorphism, GSA Today 11 (2001) 4–9.
[5] D.R. Montgomery, G. Balco, S.D. Willett, Climate, tectonics, and the morphology of the Andes, Geology (2001) 579–582.
[6] S.J. Dadson, N. Hovius, H. Chen, W.B. Dade, M-L. Hsieh, S.D. Willett, J-C. Hu, M-J. Horng, M-C. Chen, C.P. Stark, D. Lague, J.-.C. Lin, Links between erosion, runoff variability and seismicity in the Taiwan orogen, Nature 426 (2003) 648–651.
[7] P.W. Reiners, T.A. Ehlers, S.G. Mitchell, D.R. Montgomery, Coupled spatial variations in precipitation and long-term erosion rates across the Washington Cascades, Nature 426 (2003) 645–647.
[8] P. Molnar, Nature, nurture and landscape, Nature 426 (2003) 612–614.
[9] K.X. Whipple, B.J. Meade, Orogen response to changes in climatic and tectonic forcing, Earth Planet. Sci. Lett. 243 (2006) 218–228.
[10] K.V. Hodges, C. Wobus, K. Ruhl, T. Schildgen, K. Whipple, Quaternary deformation, river steepening, and heavy precipitation at the front of the Higher Himalayan ranges, Earth Planet. Sci. Lett. 220 (2004) 379–389.
[11] C. Wobus, A. Heimsath, K. Whipple, K. Hodges, Active out-of-sequence thrust faulting in the central Nepalese Himalaya, Nature 434 (2005) 1008–1011.
[12] D.W. Burbank, Cracking the Himalaya, Nature 434 (2005) 963–964.
[13] J. Lavé, J.P. Avouac, Fluvial incision and tectonic uplift across the Himalayas of central Nepal, J. Geophys. Res. 106 (2001) 26561–26591.
[14] D.W. Burbank, A.E. Blythe, J. Putkonen, B. Pratt-Sitaula, E. Gabet, M. Oskin, A. Barros, T.P. Ojha, Decoupling of erosion and precipitation in the Himalayas, Nature 426 (2003) 652–655.
[15] C.W. Wobus, K.V. Hodges, K.X. Whipple, Has focused denudation sustained active thrusting at the Himalayan topographic front? Geology 31 (2003) 861–864.
[16] A.P. Barros, M. Joshi, J. Putkonen, D.W. Burbank, A study of the 1999 monsoon rainfall in central Nepal using TRMM products and rain gauge observations, Geophys. Res. Lett. 27 (2000) 3683–3686.
[17] T.J. Lang, A.P. Barros, An investigation of the onsets of the 1999 and 2000 monsoons in central Nepal, Mon. Weather Rev. 130 (2002) 1299–1316.
[18] J.K. Putkonen, Continuous snow and rain data at 500 to 4400 m altitude near Annapurna, Nepal, 1999–2001, Arct. Antarct. Alp. Res. 36 (2004) 244–248.
[19] E.J. Gabet, B.A. Pratt-Sitaula, D.W. Burbank, Climatic controls on hillslope angle and relief in the Himalayas, Geology 32 (2004) 629–632.

[20] B. Pratt-Sitaula, D.W. Burbank, A.M. Heimsath, T. Ojha, Landscape disequilibrium on 1000–10,000 year scales, Marsyandi River, Nepal, central Himalaya, Geomorphology 58 (2004) 223–241.
[21] A. Galy. 1999. Étude géochimique de l' érosion actuelle de la chaîne himalayenne, Thèse de Doctorat, CRPG Nancy, 464.
[22] A. Galy, C. France-Lanord, Weathering processes in the Ganges–Brahmaputra basin and the riverine alkalinity budget, Chem. Geol. 159 (1999) 31–60.
[23] A. Galy, C. France-Lanord, L.A. Derry, The strontium isotopic budget of Himalayan Rivers in Nepal and Bangladesh, Geochim. Cosmochim. Acta 63 (1999) 1905–1925.
[24] E.T. Tipper, M.J. Bickle, A. Galy, A.J. West, C. Pomiès, H.J. Chapman, The short term climatic sensitivity of carbonate and silicate weathering fluxes: insight from seasonal variations in river chemistry, Geochim. Cosmochim. Acta 70 (2006) 2737–2754.
[25] E.J. Gabet, D.W. Burbank, J.K. Putkonen, B.A. Pratt-Sitaula, T. Ojha, Rainfall thresholds for landsliding in the Himalayas of Nepal, Geomorphology 63 (2004) 131–143.
[26] M. Attal, J. Lavé, Changes of bedload characteristics along the Marsyandi River (central Nepal): implications for understanding hillslope sediment supply, sediment load evolution along fluvial networks, and denudation in active orogenic belts, Geol. Soc. Am., Spec. Pap. 398 (2006) 143–171.
[27] K.W. Huntington, A.E. Blythe, K.V. Hodges, Climate change and Late Pliocene acceleration of erosion in the Himalaya, Earth Planet. Sci. Lett. 252 (2006) 107–118.
[28] A.E. Blythe, D.W. Burbank, A. Carter, K.L. Schmidt, J. Putkonen, Plio-Quaternary exhumation history of the central Nepalese Himalaya: 1. Apatite and zircon fission-track and apatite (U/Th)/He analyses, Tectonics (in press), doi:10.1029/2006TC001990.
[29] N.A. Niemi, M. Oskin, D.W. Burbank, A.M. Heimsath, E.J. Gabet, Effects of bedrock landslides on cosmogenically determined erosion rates, Earth Planet. Sci. Lett. 237 (2005) 480–498.
[30] A.M. Heimsath, C. Wobus, Erosion rates and processes across two trans-Himalayan transects in central Nepal, AGU Fall Meeting 12/2004, 2004, Abstract.
[31] I.D. Brewer, D.W. Burbank, K.V. Hodges, Modelling detrital cooling-age populations: insights from two Himalayan catchments, Basin Res. 15 (2003) 305–320.
[32] K.W. Ruhl, K.V. Hodges, The use of detrital mineral cooling ages to evaluate steady state assumptions in active orogens: an example from the central Nepalese Himalaya, Tectonics 24 (2005) TC4015.
[33] I.D. Brewer, D.W. Burbank, K.V. Hodges, Downstream development of a detrital cooling-age signal: insights from $^{40}Ar/^{39}Ar$ muscovite thermochronology in the Nepalese Himalaya, Geol. Soc. Am., Spec. Pap. 398 (2006) 321–338.
[34] W.H. Amidon, D.W. Burbank, G.E. Gehrels, Construction of detrital mineral populations: insights from mixing of U–Pb zircon ages in Himalayan rivers, Basin Res. 17 (2005) 463–485.
[35] W.H. Amidon, D.W. Burbank, G.E. Gehrels, U–Pb zircon ages as a sediment mixing tracer in the Nepal Himalaya, Earth Planet. Sci. Lett. 235 (2005) 244–260.
[36] B. Bookhagen, R.C. Thiede, M.R. Strecker, Abnormal monsoon years and their control on erosion and sediment flux in the high, arid northwest Himalaya, Earth Planet. Sci. Lett. 231 (2005) 131–146.
[37] M. Colchen, P. Le Fort, A. Pêcher, Annapurna, Manaslu, Ganesh Himal (with 1:200.000 geological map), Paris, Éditions du CNRS, 1986, 136 pp.
[38] L. Godin, T. Gleeson, M.P. Searle, T.D. Ullrich, R.R. Parrish, Locking of southward extrusion in favour of rapid crustal-scale buckling of the Greater Himalayan sequence, Nar valley, central Nepal, in: R. Law, M.P. Searle, L. Godin (Eds.), Channel flow, ductile extrusion and exhumation in continental collision zones, Geol. Soc. London Spec. Publ., vol. 268, 2006, pp. 269–292.
[39] E. Garzanti, Stratigraphy and sedimentary history of the Nepal Tethys Himalayan passive margin, J. Asian Earth Sci. 17 (1999) 805–827.
[40] C. Schneider, L. Masch, The metamorphism of the Tibetan Series from the Manang area, Marsyandi Valley, Central Nepal, in: P.J. Treloar, M.P. Searle (Eds.), Himalayan tectonics, Geol. Soc. London, Spec. Publ., vol. 74, 1993, pp. 357–374.
[41] E. Garzanti, M. Gorza, L. Martellini, A. Nicora, Transition from diagenesis to metamorphism in the Paleozoic to Mesozoic succession of the Dolpo-Manang Synclinorium and Thakkhola Graben (Nepal Tethys Himalaya), Eclogae Geol. Helv. 87 (1994) 613–632.
[42] T.M. Harrison, M. Grove, K.D. McKeegan, C.D. Coath, O.M. Lovera, P. Le Fort, Origin and episodic emplacement of the Manaslu intrusive complex, J. Petrol. 40 (1999) 3–19.
[43] R.V. Ingersoll, Actualistic sandstone petrofacies: discriminating modern and ancient source rocks, Geology 18 (1990) 733–736.
[44] R.V. Ingersoll, T.F. Bullard, R.L. Ford, J.P. Grimm, J.D. Pickle, S.W. Sares, The effect of grain size on detrital modes: a test of the Gazzi–Dickinson point-counting method, J. Sediment. Petrol. 54 (1984) 103–116.
[45] E. Garzanti, G. Vezzoli, A classification of metamorphic grains in sands based on their composition and grade, J. Sediment. Res. 73 (2003) 830–837.
[46] E. Garzanti, S. Andò, Heavy mineral concentration in modern sands: implications for provenance interpretation, in: M. Mange, D. Wright (Eds.), Heavy Minerals in Use, Developments in Sedimentology Series, vol. 58, Elsevier, Amsterdam, 2007, pp. 567–598.
[47] G.J. Weltje, End-member modelling of compositional data: numerical–statistical algorithms for solving the explicit mixing problem, J. Math. Geol. 29 (1997) 503–549.
[48] G. Einsele, M. Hinderer, Terrestrial sediment yield and the lifetimes of reservoirs, lakes, and larger basins, Geol. Rundsch. 86 (1997) 288–310.
[49] E. Garzanti, G. Vezzoli, P. Paparella, P.D. Clift, Petrology of Indus River sands: a key to interpret erosion history of the Western Himalayan Syntaxis, Earth Planet. Sci. Lett. 229 (2005) 287–302.
[50] M.J. Johnsson, The system controlling the composition of clastic sediments, in: M.J. Johnsson, A. Basu (Eds.), Processes controlling the composition of clastic sediments, Geol. Soc. Am. Spec. Pap., vol. 284, 1993, pp. 1–19.
[51] G.J. Weltje, H. Von Eynatten, Quantitative provenance analysis of sediments: review and outlook, Sediment. Geol. 171 (2004) 1–11.
[52] H.W. Nesbitt, G.M. Young, Petrogenesis of sediments in the absence of chemical weathering: effects of abrasion and sorting on bulk composition and mineralogy, Sedimentology 43 (1996) 341–358.
[53] E. Garzanti, G. Vezzoli, S. Andò, C. France-Lanord, S.K. Singh, G. Foster, Sand petrology and focused erosion in collision orogens: the Brahmaputra case, Earth Planet. Sci. Lett. 220 (2004) 157–174.
[54] A.C. Morton, C.R. Hallsworth, Processes controlling the composition of heavy mineral assemblages in sandstones, Sediment. Geol. 124 (1999) 3–29.

[55] G. Rittenhouse, Transportation and deposition of heavy minerals, Geol. Soc. Amer. bull. 54 (1943) 1725–1780.
[56] M.A. Summerfield, N.J. Hulton, Natural controls of fluvial denudation rates in major world drainage basins, J. Geophys. Res. 99 (1994) 13871–13883.
[57] His Majesty's Government (HMG) of Nepal, Middle Marsyandi Hydroelectric Project, Nepal Electr. Author., August 1994.
[58] His Majesty's Government (HMG) of Nepal, Feasibility study on Sapt Gandaki hydroelectric power development project, Nepal Electr. Author., April 1982.
[59] R. Sinha, P.F. Friend, River systems and their sediment flux, Indo-Gangetic plains, Northern Bihar, India, Sedimentology 41 (1994) 825–845.
[60] E. Garzanti, S. Ando', G. Vezzoli, The continental crust as a source of sand (Southern Alps cross-section, Northern Italy), J. Geol. 114 (2006) 533–554.
[61] I.M. Villa, From nanometer to megameter: isotopes, atomic-scale processes, and continent-scale tectonic models, Lithos 87 (2006) 155–173.
[62] J.T. Harper, N.F. Humphrey, High altitude Himalayan climate inferred from glacial ice flux, Geophys. Res. Lett. 30 (2003) 14, 1764, doi:10.1029/2003GL017329.
[63] N. Brozovic, D.W. Burbank, A.J. Meigs, Climatic limits on landscape development in the Northwest Himalaya, Science 276 (1997) 571–574.
[64] V. Godard, R. Cattin, J. Lavé, Numerical modeling of mountain building: interplay between erosion law and crustal rheology, Geophys. Res. Lett. 31 (2004) L23607, doi:10.1029/2004GL021006.
[65] W.R. Dickinson, Interpreting provenance relations from detrital modes of sandstones, in: G.G. Zuffa (Ed.), Provenance of arenites, ASI Series, vol. 148, Reidel, Dordrecht, 1985, pp. 333–361.
[66] G.J. Weltje, Quantitative analysis of detrital modes: statistically rigorous confidence methods in ternary diagrams and their use in sedimentary petrology, Earth Sci. Rev. 57 (2002) 211–253.